analytical chemistry

pubs.acs.org/ac Article

Electrochemical Immunosensor for Cardiac Troponin I Detection Based on Covalent Organic Framework and Enzyme-Catalyzed Signal Amplification

Sinuo Feng, Mengxia Yan, Yu Xue, Jianshe Huang,* and Xiurong Yang*

Cite This: *Anal. Chem.* 2021, 93, 13572−13579 Read Online

ACCESS | Metrics & More | Article Recommendations | Supporting Information

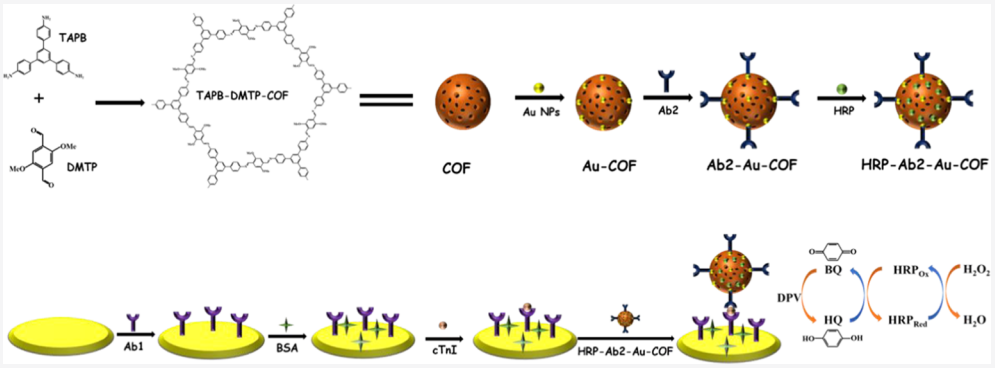

ABSTRACT: Herein, a highly sensitive electrochemical immunosensor was presented for the cardiac troponin I (cTnI) determination using a multifunctional covalent organic framework-based nanocomposite (HRP-Ab2-Au-COF) as the signal amplification probe. The spherical COF with a large surface area was synthesized in a short time by a simple solution-based method at room temperature. The good biocompatibility, low toxicity, and high stability in water of the COF guarantee its application in biosensing. Besides, its high porosity makes it an excellent carrier for loading abundant horseradish peroxidase (HRP). The modified gold nanoparticles on the surface of COF not only provide a load platform for secondary antibody (Ab2) but also improve the conductivity of COF. Under the synergistic effect of the hydrogen peroxide (H_2O_2) and HRP, hydroquinone (HQ) in the solution is catalytically oxidized to benzoquinone (BQ), which is then reduced on the electrode surface to generate the electrochemical signal. The designed probes not only show the specific recognition behavior of Ab2 to cTnI but also improve the sensitivity of the biosensing system due to the signal amplification caused by the excellent enzyme catalytic performance of HRP. Based on the H_2O_2-HRP-HQ signal amplification system, the biosensor for cTnI was fabricated and exhibited a linear response as a function of logarithmic cTnI concentration ranging from 5 pg/mL to 10 ng/mL, and the detection limit was 1.7 pg/mL. Moreover, the biosensor exhibited excellent recovery and reproducibility in the actual sample testing. This work provided a simple approach to determine cTnI quantitatively in practical samples and broadened the utilization scope of the COF-based nanocomposite in the electrochemical immunosensor.

1. INTRODUCTION

Acute myocardial infarction (AMI) is the most serious kind of coronary heart disease and causes a severe threat to human health.[1,2] Up to now, creatine kinase-MB, myoglobin, C-reactive protein, and cTnI are valuable biomarkers for the diagnosis of AMI.[3] Among them, cTnI is the most specific and longest window period biomarker in clinical use,[4,5] which is thought to be the gold standard of AMI diagnosis. Consequently, it is critical to develop a fast and sensitive analytical approach to detect cTnI.

Immunological detection based on the high specific identification of between antigen and antibody is an important analytical method in qualitative and quantitative detection of biomarkers. At present, many immunoassay methods based on enzyme-linked immunosorbent assay, such as chemiluminescence immunoassay, fluorescence, surface-enhanced Raman scattering, and colorimetry, have been applied to cTnI detection.[6−10] Compared with the above methods, electrochemical immunosensors have aroused considerable concern owing to virtues of quick response, splendid selectivity, high sensitivity, and simple operation.[11−15] In recent years, various

Received: June 23, 2021
Accepted: September 16, 2021
Published: September 30, 2021

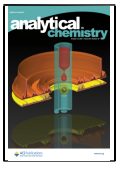

nanomaterials have been used to devise electrochemical immunosensors of cTnI to enhance detection sensitivity. For example, Yan et al.[16] used the functional carbon nanotube composite with a large electroactive surface area and splendid electrocatalytic activity to increase the sensitivity of the electrochemical sensor. Lv et al.[17] achieved high sensitive determination of cTnI using the core−shell bimetallic multibranched nanoparticles as the conductive substrate material and functionalized graphene oxide as the double signal label. Chen et al.[18] designed multimetallic superstructured nanocrystals PtCoCuPd as a signal amplification probe to detect cTnI. Therefore, it is significant and urgent to design novel functional nanomaterials and to build electrochemical immunosensors for fast, selective, and sensitive determination of cTnI.

The covalent organic framework (COF) is a kind of material that links organic structural units together by covalent bonds to form a porous crystalline framework with periodic structures.[19] It has many unique advantages including large surface area, adjustable pore size, high porosity, low toxicity, good biocompatibility, and so on. Therefore, COFs have been used in many areas of research, such as drug delivery, separation, catalysis, and gas adsorption and storage, etc.[20−28] In recent years, COFs with unique porous, electronic and mechanical properties have been functionalized with other electroactive materials to design various signal amplification strategies for improving the analytical performance of electrochemical immunosensors.[29,30] However, the development of COF-based electrochemical immunosensor for cTnI is still in its infancy.[31]

Based on the above background, we designed a COF-based signal probe, which was used to the sandwich-type electrochemical immunoassay of cTnI for the first time. The constructed electrochemical signal probe HRP-Ab2-Au-COF integrated the functions of target recognition and signal amplification, and the gold nanoparticles loading on the surface of COF enhanced the conductivity and facilitated the binding of the antibody (Ab2). When the target cTnI was introduced, HRP-Ab2-Au-COF was immobilized on the electrode surface via antibody−antigen interaction, where the H_2O_2-HRP system catalytically oxidized hydroquinone (HQ) to produce benzoquinone (BQ) that was further reduced to generate an electrochemical signal. This biosensor exhibited great analytical performance for cTnI with the detection limit of 1.7 pg/mL and satisfactory detection results in real samples, demonstrating its outstanding application prospect for the determination of target proteins in clinical analysis.

2. EXPERIMENTAL SECTION

2.1. Reagents. 1,3,5-Tris(4-aminophenyl)benzene (TAPB) and 2,5-dimethoxyterephaldehyde (DMTP) were obtained from Jilin Chinese Academy of Sciences-Yanshen Technology Co., Ltd. Acetonitrile (CH_3CN), sodium borohydride ($NaBH_4$), glucose oxidase (GOx), hemoglobin (Hb), immunoglobulin G (IgG), and horseradish peroxidase (HRP) were supplied by Sigma-Aldrich. Hydrogen tetrachloroaurate-(III) hydrate ($HAuCl_4{\cdot}4H_2O$) was purchased from Strem Chemicals. Bovine serum albumin (BSA) and hydroquinone (HQ) were bought from Sangon Biotechnology Co., Ltd. Acetic acid (CH_3COOH), hydrogen peroxide (H_2O_2), and ethanol (CH_3CH_2OH) were provided by Xilong Scientific. The cardiac troponin (cTnI and cTnT) and cTnI antibody (Ab1 and Ab2) were purchased from Abcam (Cambridge, MA). The phosphate buffer solution I (PBSI, pH 7.4, 0.1 M) and washing phosphate buffer solution II (PBSII, pH 7.4, 0.01 M) were prepared from Na_2HPO_4 and NaH_2PO_4. Millipore ultrapure water (18.25 MΩ·cm) was used throughout the experiment.

2.2. Apparatus. The transmission electron microscopy (TEM) images were acquired by a TECNAI F20 microscope operated at 200 kV. The scanning electron microscopy (SEM) images were obtained on OXFORD Instrument XMAX with a 20 kV accelerating voltage. The Fourier transform infrared (FT-IR) spectra were carried out on a Bruker VERTEX70 spectrometer within the scope of 500−4000 cm^{-1} (Ettlingen, Germany). The X-ray photoelectron spectroscopy (XPS) measurements were taken on an ESCALAB MK II spectrometer (VG Scientific) using Al Kα as the radiation. The X-ray diffraction (XRD) was performed on a D8 ADVANCE diffractometer (Bruker, Germany) with a Cu Ka radiation (λ = 0.154 nm). Dynamic light scattering (DLS) and Zeta potential were measured with a Zetasizer Nano ZS system (Malvern, England) at 25 °C. The Brunauer−Emmett−Teller (BET) surface area, pore volume, and pore size were obtained on Autosorb iQ Station with liquid N_2 as an adsorbent at 77 K. The element composition was measured by inductively coupled plasma-optical emission spectrometry (ICP-OES, Thermo ICAP 6300).

2.3. Synthesis of Materials. The COF was synthesized on the basis of the published literature with a slight change.[32] TAPB (4 mg, 0.0112 mmol) and DMTP (4 mg, 0.024 mmol) were dissolved in 8 mL of CH_3CN with ultrasonication for 30 s. Then, 0.2 mL of acetic acid was injected into the mixed solution under vigorous stirring and continued to stir for 24 h at room temperature. The yellow sediment was collected by centrifugation and washed with ethanol two times and then dried under a vacuum at 50 °C.

Au-COF was synthesized as follows. First, the as-prepared COF (1 mg) was ultrasonically dispersed in 1 mL of ultrapure water for 10 min. Then, $HAuCl_4$ aqueous solution (0.2 mL, 1.5 mg/mL) was injected into the dispersion under stirring. After stirring for 4 h, 0.2 mL of $NaBH_4$ solution (2 mg/mL) was rapidly injected into the above solution and continued to stir for another 2 h. The precipitate was collected and washed with deionized water three times. Afterward, the prepared Au-COF was dried under a vacuum at 50 °C.

To obtain HRP-Ab2-Au-COF, 10 μL of Ab2 (0.9 mg/mL) was injected into the above-prepared Au-COF solution (1 mL, 1 mg/mL) with agitation at 4 °C for 3 h. Afterward, HRP (1 mL, 1 mg/mL) was injected into the solution and then continued to stir for 12 h at 4 °C. Then, 100 μL of BSA (1%) was injected into the mixture solution and continued to stir for 1 h at 4 °C to block the excessive binding sites. The resultant product was centrifuged and washed with deionized water and finally dispersed in 1 mL of PBSII and stored at 4 °C for further use.

2.4. Preparation of the Modified Electrodes. The pretreatment procedure of the GE was as follows. First, the bare GE was immersed in piranha solution for 20 min to clean the surface preliminarily. Afterward, the electrode was polished successively with alumina slurry (1.0, 0.3, and 0.05 μm) and then cleaned exhaustively by ultrasonic treatment in ethanol and ultrapure water. Finally, the electrochemical activation of bare GE was carried out in 0.5 M H_2SO_4 solution until the characteristic cyclic voltammetry (CV) curve was obtained.

https://doi.org/10.1021/acs.analchem.1c02636
Anal. Chem. 2021, 93, 13572−13579

Scheme 1. Schematic Illustration of the Synthesis of HRP-Ab2-Au-COF and the Constructive Procedure of the Biosensor for cTnI Detection

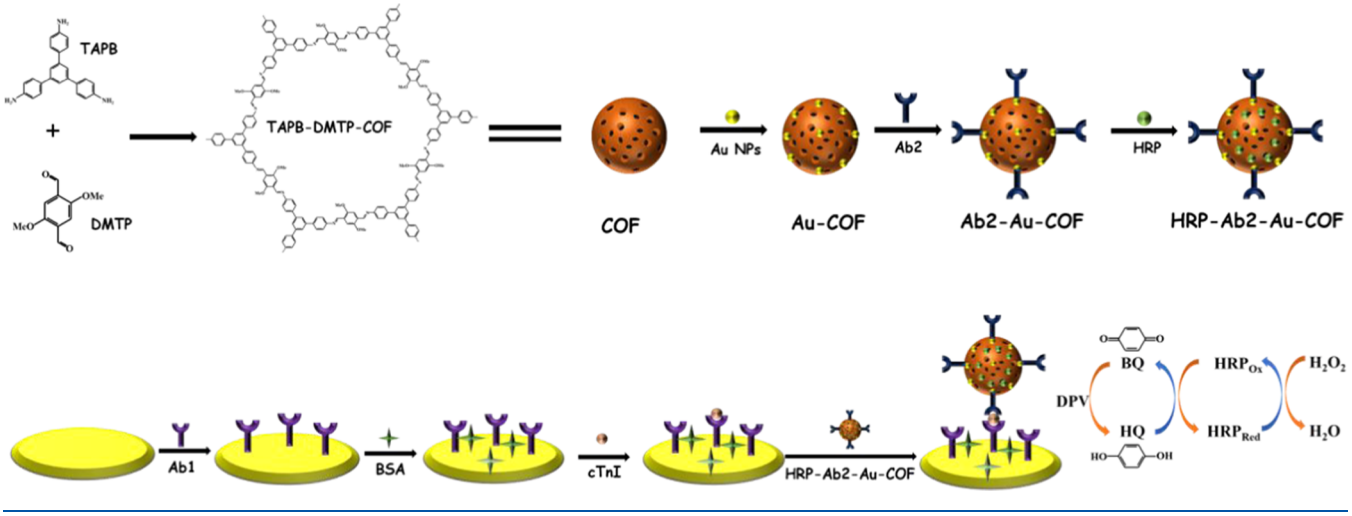

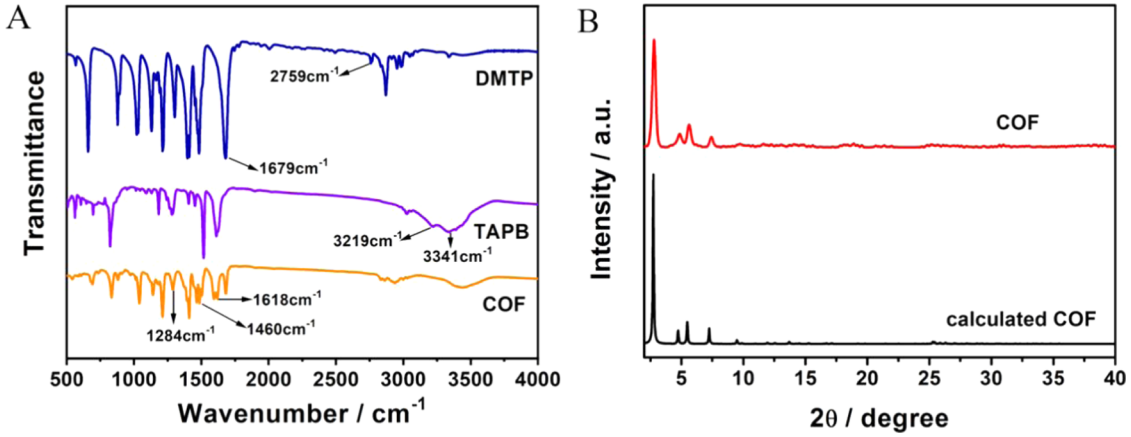

Figure 1. (A) FT-IR spectra of the COF and its corresponding precursors. (B) Calculated and experimental XRD patterns of the COF.

Finally, the electrode was rinsed with ultrapure water and dried with nitrogen before use.

To prepare the modified electrode, 8 μL of Ab1 (10 μg/mL) was loaded onto the electrode surface and incubated at 4 °C for 12 h. Subsequently, 4 μL of BSA (1%) solution was added onto the electrode for 40 min to block the nonspecific sites. Next, 8 μL of the cTnI solution with various concentrations was placed on the surface of the modified electrode at 37 °C for 90 min. Finally, the above-modified electrode was incubated with the prepared aqueous dispersion of HRP-Ab2-Au-COF bioconjugate for 1 h at 37 °C. After every modification step, the electrode was carefully rinsed with 3 times the volume of PBSII to remove weakly bound components.

2.5. Measurements. All electrochemical experiments were carried out with a CHI660E (Chenhua Instruments, Shanghai, China) electrochemical workstation with a traditional three-electrode system, which is composed of a modified gold electrode (GE) (Φ = 3 mm) as the working electrode, a platinum wire as the counter electrode, and an Ag/AgCl (saturated with KCl) as the reference electrode. Electrochemical impedance spectroscopy (EIS) and CV were measured in 0.1 M KCl solution containing 5 mM $[Fe(CN)_6]^{3-/4-}$. The frequency range of EIS was 0.1 Hz−100 kHz. The applied potential range for CV measurement was from −0.2 to 0.6 V with scan rate of 100 mV/s. For cTnI measurement, the differential pulse voltammetry (DPV) was conducted in 0.1 M PBSI (pH 7.4) containing HQ and H_2O_2. The experimental parameters of DPV were as follows: initial potential 0.2 V, final potential −0.25 V, pulse height 50 mV, step height 4 mV, and pulse width 0.05 s. All of the electrochemical experiments were carried out at room temperature. To detect cTnI in human serum, the human serum sample was diluted 20-fold using PBSII (pH 7.4) buffer. Then, the standard addition method was used to evaluate the practical applicability according to the above procedures under the optimized condition.

3. RESULTS AND DISCUSSION

3.1. Principle of the Sensing Method. Scheme 1 briefly illustrates the preparation procedure of HRP-Ab2-Au-COF, and the assembly procedure of the electrochemical immunosensor. At first, the spherical COF was prepared by TAPB and DMTP at room temperature via an uncomplicated solution-phase synthesis method, and the gold nanoparticles grew in situ on the surface of the COF under the reduction of $NaBH_4$ through Au-NH_2 binding.[33,34] Then, Ab2 was combined with the gold nanoparticles through the Au-NH_2 reaction. Afterward, the HRP was embedded in the pore of COF via the host−guest interaction.[35] Notably, the COF played an

https://doi.org/10.1021/acs.analchem.1c02636
Anal. Chem. 2021, 93, 13572−13579

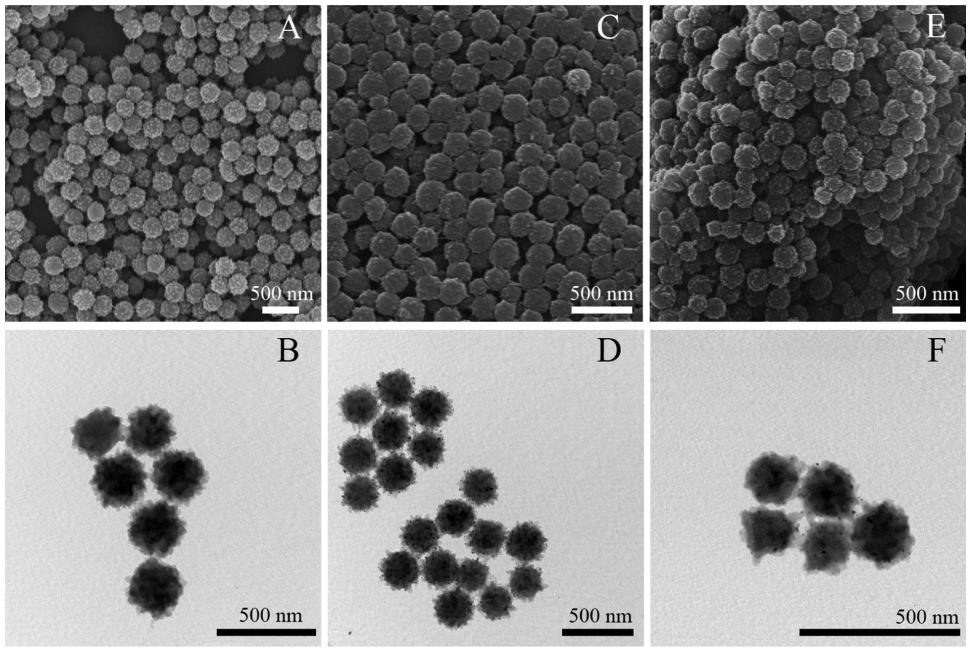

Figure 2. SEM and TEM images of (A, B) COF, (C, D) Au-COF, and (E, F) HRP-Ab2-Au-COF.

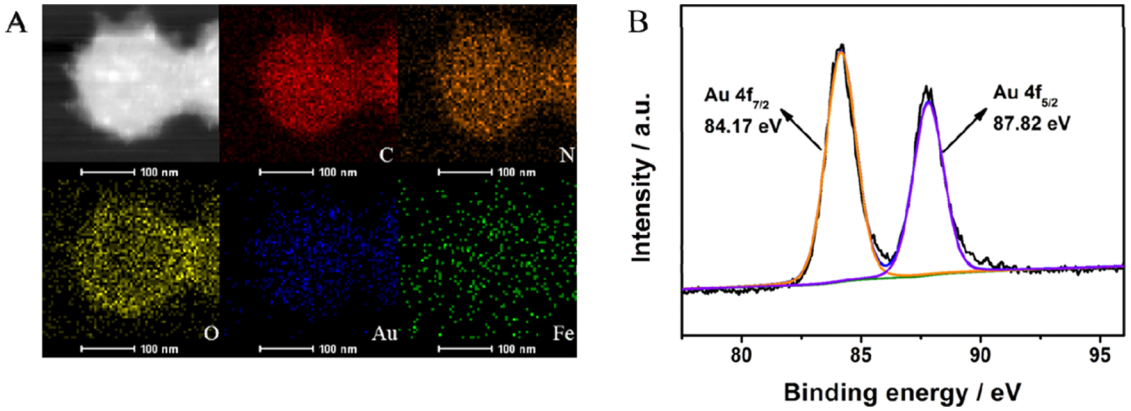

Figure 3. (A) Elemental mapping images and (B) high-resolution Au 4f region in the XPS spectrum of HRP-Ab2-Au-COF.

important role in linking gold nanoparticles, Ab2, and HRP. Furthermore, the gold nanoparticles possess excellent electrical conductivity, which can raise the sensitivity of the biosensor.[36] Due to the high porosity of COF, a large number of HRP molecules were introduced to the nanocomposite, which realized the transformation mode of the label from one-for-one to one-for-many. The combination of HRP and Ab2-labeled COF can simultaneously achieve target recognition and signal amplification.

For the detection of cTnI, capture antibody Ab1 was first immobilized on the surface of bare GE via the Au-NH_2 binding. After blocking the excess active sites by BSA, the modified electrode was incubated with different concentrations of cTnI. Finally, the as-prepared HRP-Ab2-Au-COF bioconjugate was captured by cTnI. After immersing the modified electrode into the electrolyte, H_2O_2 could effectively oxidize HRP to HRP_{Ox}, which further oxidized HQ to BQ and regenerated HRP_{Red}.[37] Next, the BQ was reduced around the electrode surface and generated an obvious electrochemical signal. Through this H_2O_2-HRP-HQ catalytic cycle, the amplified current signal could be acquired and the designed biosensor applied to the quantitative detection of cTnI.

3.2. Characterization of Materials. The COF was synthesized by binding TAPB with DMTP through aldimine condensation. The FT-IR spectra of DMTP, TAPB, and COF are shown in Figure 1A. The characteristic peak of DMTP at 1679 cm^{-1} was ascribed to the stretching vibration of C═O, and the peak at 2759 cm^{-1} was the vibration of C−H in the aldehyde group.[35] The peaks of TAPB at 3219 and 3341 cm^{-1} were attributed to the vibration of N−H. For COF, the characteristic absorption peaks appeared at 1618, 1284, and 1460 cm^{-1}, which were attributed to the stretching vibration of C═N, C−O, and $-CH_3$, respectively, accompanying the decrease of the aldehyde stretching vibration peak of DMTP and amino stretching vibration peak of TAPB. The above FT-IR analysis results showed that a condensation reaction had occurred.[38] Furthermore, the XRD pattern of the as-synthesized COF (Figure 1B) revealed a strong peak at 2.78° and several comparatively small peaks at 4.86, 5.57, and 7.38°, respectively, which agreed well with the calculated pattern.[39,40] Both FT-IR and XRD results confirmed the preparation of the highly crystalline COF.

SEM and TEM were used to characterize the morphology of COF materials (Figure 2). The COF showed uniform spherical

https://doi.org/10.1021/acs.analchem.1c02636
Anal. Chem. 2021, 93, 13572−13579

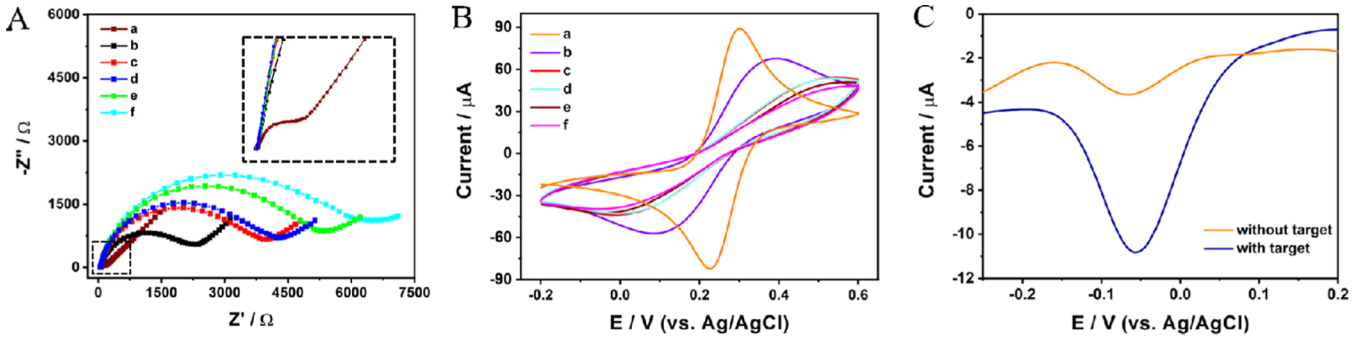

Figure 4. (A) Nyquist plots and (B) CV curves of (a) bare GE, (b) Ab1/GE, (c) BSA/Ab1/GE, (d) HRP-Ab2-Au-COF/BSA/Ab1/GE, (e) cTnI/BSA/Ab1/GE, and (f) HRP-Ab2-Au-COF/cTnI/BSA/Ab1/GE in 0.1 M KCl aqueous solution containing 5 mM $[Fe(CN)_6]^{3-/4-}$, scan rate 100 mV/s. (C) DPV responses of the proposed biosensor toward 1 ng/mL cTnI and without a target in the PBSI solution including 3 mM HQ and 2 mM H_2O_2.

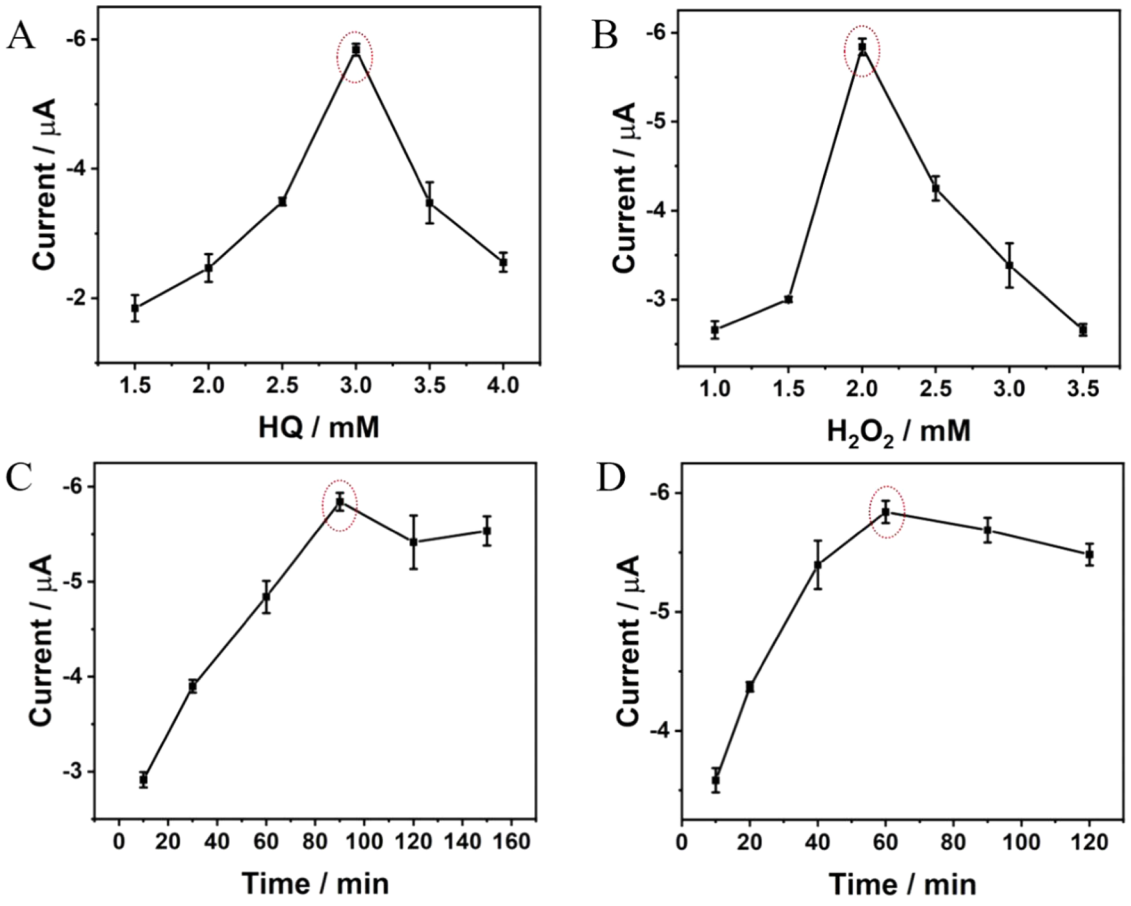

Figure 5. Optimization of the experimental parameters. The concentrations of (A) HQ and (B) H_2O_2 and the incubation times of (C) cTnI and (D) HRP-Ab2-Au-COF.

morphology with a rough surface (Figure 2A,B) and its diameter was about 256 nm (Figure S3). The gold nanoparticles grown in situ on COF were about 2.5 nm in size and distributed uniformly (Figure 2D,F). It was noteworthy that the morphology (Figure 2C−F) of Au-COF and HRP-Ab2-Au-COF remained unchanged compared with COF after the growth of gold nanoparticles and loading with proteins. However, compared with COF (294.1 nm), the hydrodynamic size of Au-COF and HRP-Ab2-Au-COF gradually increased to 336.6 and 423.7 nm, respectively. Meanwhile, the corresponding Zeta potential also became more and more negative (Figures S4, S5, and Table S1). Additionally, the surface area, average pore size, and pore volume of the synthesized COF were analyzed by measuring the nitrogen adsorption−desorption isotherm at 77 K (Figures S1 and S2). The BET surface area of the COF was calculated to be 386.7 m^2/g. In addition, according to the NLDFT analysis, the pore volume and average pore size of the COF were about 0.56 cm^3/g and 2.88 nm, respectively.[41]

The elemental mapping of HRP-Ab2-Au-COF showed the homogeneous dispersion of Au and Fe (Figure 3A), demonstrating that the Au nanoparticles and HRP were successfully combined with the COF. The XPS spectrum of Au 4f is displayed in Figure 3B. The two peaks at 84.17 and 87.82

https://doi.org/10.1021/acs.analchem.1c02636
Anal. Chem. 2021, 93, 13572−13579

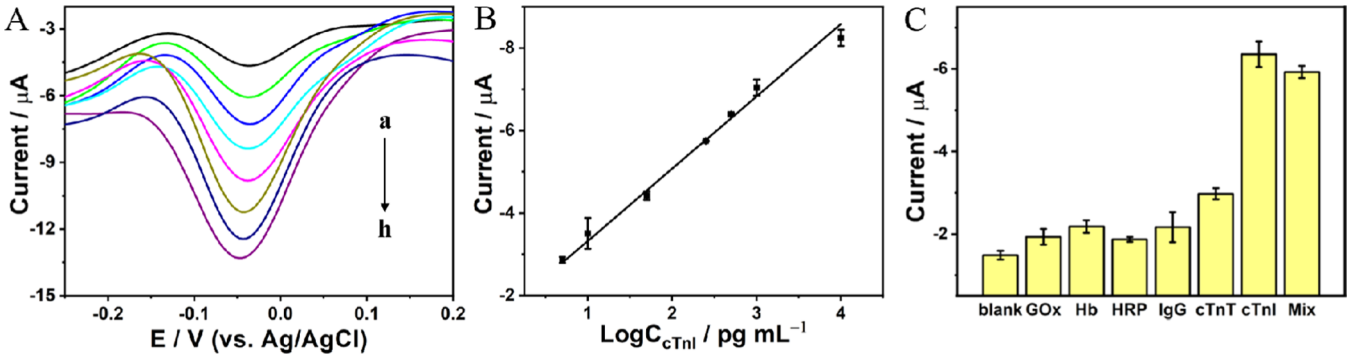

Figure 6. (A) DPV response curves of the presented electrochemical immunosensor (concentration of cTnI from a to h: 0−10 ng/mL) and (B) the resulting linear relationship between the current and the logarithm of cTnI concentration. (C) Specificity of the biosensor at 1 ng/mL of cTnI and other interfere proteins (10 ng/mL).

eV were attributed to Au $4f_{7/2}$ and $4f_{5/2}$, respectively.[42] In light of the ICP-OES result, the contents of Au and Fe were about 7.62 and 0.063%, respectively. All of the above analysis results confirmed the successful synthesis of HRP-Ab2-Au-COF nanocomposites.

3.3. Feasibility of the Sensing Method. To make sure the feasibility of the sensing method, CV and EIS experiments were performed to investigate the electrode modification procedure. As displayed in Figure 4A, the bare GE exhibited a pretty small semicircle, which proved its outstanding conductivity. After immobilizing Ab1, blocking with BSA, and capturing the cTnI, the charge-transfer resistance (R_{ct}) increased successively, which was due to the curbing of the electron transfer by nonelectroactive proteins. Subsequently, the R_{ct} further increased after binding with the HRP-Ab2-Au-COF bioconjugate. Additionally, in the absence of cTnI, the modified electrode incubated with HRP-Ab2-Au-COF showed similar R_{ct} to that of BSA/Ab1/GE (curve d), indicating that negligible HRP-Ab2-Au-COF bioconjugate nonspecifically adsorbed on the electrode surface. The corresponding CV curves in Figure 4B show the decreased peak current and increased peak-to-peak separation after stepwise modification of Ab1, BSA, cTnI, and HRP-Ab2-Au-COF, which was coincided with the result of EIS. Additionally, Figure 4C shows the DPV curves of the presented electrochemical biosensor with or without target cTnI in the PBSI solution containing HQ and H_2O_2. In the absence of cTnI, the biosensor showed a small current response at −0.064 V. However, with the addition of 1 ng/mL target cTnI, the current significantly increased by 4.6 times due to the H_2O_2-HRP-HQ-mediated signal amplification. These results proved the successful assembly and feasibility of the proposed biosensor.

3.4. Analytical Performances of the Biosensor. To fulfill the optimal analysis performance of the developed biosensor, several experimental conditions, including the concentrations of HQ and H_2O_2 and the incubation times of cTnI and HRP-Ab2-Au-COF, were investigated with 1 ng/mL of cTnI as a model. As illustrated in Figure 5A,B, the maximum current responses were obtained when the optimal concentration of HQ and H_2O_2 were 3.0 and 2.0 mM, respectively. The electrochemical response current first increased with the incubation time between cTnI and BSA/Ab1/GE, and then reached the maximum when the incubation time was 90 min (Figure 5C). Besides, the current response also increased with the enhancement of the binding time between HRP-Ab2-Au-COF and cTnI/BSA/Ab1/GE, and the maximum current was obtained after 60 min of incubation (Figure 5D). Therefore, 90 and 60 min were chosen as the optimum combined time for cTnI and HRP-Ab2-Au-COF, respectively.

Under optimal experimental conditions, the concentrations of cTnI were investigated by measuring the DPV response current. As we can see from Figure 6A,B, the DPV current signals of the biosensor enhanced with the increasing concentrations of cTnI. The response current was linear with the logarithm of cTnI concentration ranging from 5 pg/mL to 10 ng/mL, with the correlation coefficient of 0.9918. Meanwhile, the limit of detection was calculated to be 1.7 pg/mL (S/N = 3). In clinical study, the concentration of cTnI from 0.5 to 2.0 ng/mL is deemed as the demarcation line between normal people and patients.[43] Accordingly, this method can be applied to detect cTnI in real samples. Besides, our proposed biosensor showed comparable or better analytical performance compared with other electrochemical and optimal methods for cTnI detection (Table S2).

Under the same experimental conditions, several proteins including GOx, Hb, HRP, IgG, and cTnT were also measured to study the specificity of the presented analytical approach. The analytical results are shown in Figure 6C. The investigated interferences (10 ng/mL) exhibited very low electrochemical responses, which were similar to the blank sample and markedly lower than cTnI (1 ng/mL). Additionally, the mixture solution of interfering proteins and cTnI showed a comparable peak current to that of the pure cTnI solution. These results demonstrated that the proposed biosensor possessed outstanding selectivity. The reproducibility of the biosensor was also evaluated. Five biosensors were fabricated independently to determine the 1 ng/mL cTnI solution. The relative standard deviation (RSD) of the detected DPV peak current was 2.69%, which demonstrated the excellent reproducibility of the proposed biosensing platform.

3.5. Clinical Sample Analysis. To evaluate the practical application of the developed method in the analysis of a real sample, the standard addition method was utilized to determine cTnI in 5% human serum. As listed in Table S3, the recovery ranged from 94.3 to 104.1%, and the RSD values of three parallel measurements were less than 4.73%. These results confirmed that the present method could offer a promising alternative for quantifying cTnI in biological samples.

https://doi.org/10.1021/acs.analchem.1c02636
Anal. Chem. 2021, 93, 13572−13579

4. CONCLUSIONS

In short, an electrochemical biosensing platform based on COF was constructed for the quantitative determination of cTnI. Given the advantage of high porosity, a great deal of HRP was encapsulated into the COF, which can effectively boost the oxidation of HQ to BQ with the help of H_2O_2, and then significantly amplify the electrochemical reduction signal of BQ. Meanwhile, the good biocompatibility of COF can keep the activity and stability of the enzyme. Furthermore, the gold nanoparticles grown in situ on the surface of COF not only facilitate the immobilization of Ab2 but also improve the conductivity. Combining the above merits, the electrochemical biosensor was designed and showed a wide linear range from 5 pg/mL to 10 ng/mL for the detection of cTnI, with the detection limit of 1.7 pg/mL, and also demonstrated excellent selectivity and reproducibility. The proposed immunosensor was successfully put to the real sample determination, showing good recovery and reproducibility. In summary, our constructed COF-based electrochemical immunosensor can be a general method for detecting other biomarkers.

■ ASSOCIATED CONTENT

Supporting Information

The Supporting Information is available free of charge at https://pubs.acs.org/doi/10.1021/acs.analchem.1c02636.

Nitrogen adsorption−desorption isotherms (Figure S1), pore size distribution (Figure S1), and particle size distribution histogram (Figure S3) of the synthesized COF. Zeta potentials and dynamic light scattering measurement results of COF, Au-COF, and HRP-Ab2-Au-COF (Figures S4−S5 and Table S1). Comparison of the analytical performance of the developed electrochemical biosensor with the reported methods (Table S2) and practical application of the proposed biosensor (Table S3) (PDF)

■ AUTHOR INFORMATION

Corresponding Authors

Jianshe Huang − *State Key Laboratory of Electroanalytical Chemistry, Changchun Institute of Applied Chemistry, Chinese Academy of Sciences, Changchun, Jilin 130022, China*; Phone: +86 431 85262964; Email: huangjs@ciac.ac.cn; Fax: +86 431 85689278

Xiurong Yang − *State Key Laboratory of Electroanalytical Chemistry, Changchun Institute of Applied Chemistry, Chinese Academy of Sciences, Changchun, Jilin 130022, China; University of Science and Technology of China, Hefei, Anhui 230026, China*; orcid.org/0000-0003-0021-5135; Phone: +86 431 85262056; Email: xryang@ciac.ac.cn; Fax: +86 431 85689278

Authors

Sinuo Feng − *State Key Laboratory of Electroanalytical Chemistry, Changchun Institute of Applied Chemistry, Chinese Academy of Sciences, Changchun, Jilin 130022, China; University of Science and Technology of China, Hefei, Anhui 230026, China*

Mengxia Yan − *State Key Laboratory of Electroanalytical Chemistry, Changchun Institute of Applied Chemistry, Chinese Academy of Sciences, Changchun, Jilin 130022, China; University of Science and Technology of China, Hefei, Anhui 230026, China*

Yu Xue − *State Key Laboratory of Electroanalytical Chemistry, Changchun Institute of Applied Chemistry, Chinese Academy of Sciences, Changchun, Jilin 130022, China; University of Science and Technology of China, Hefei, Anhui 230026, China*

Complete contact information is available at: https://pubs.acs.org/10.1021/acs.analchem.1c02636

Notes

The authors declare no competing financial interest.

■ ACKNOWLEDGMENTS

This work was supported by the National Natural Science Foundation of China (Nos. 22034006, 21627808, and 21721003) and the Key Research Program of Frontier Science, CAS (QYZDY-SSW-SLH019).

■ REFERENCES

(1) Lanas, F.; Avezum, A.; Bautista, L. E.; Diaz, R.; Luna, M.; Islam, S.; Yusuf, S. *Circulation* **2007**, *115*, 1067−1074.

(2) Thygesen, K.; Alpert, J. S.; Jaffe, A. S.; Simoons, M. L.; Chaitman, B. R.; White, H. D. *Circulation* **2012**, *126*, 2020−2035.

(3) Christenson, E.; Christenson, R. H. *Ann. Lab. Med.* **2013**, *33*, 309−318.

(4) Wu, A. H. B.; Apple, F. S.; Gibler, W. B.; Jesse, R. L.; Warshaw, M. M.; Valdes, R. *Clin. Chem.* **1999**, *45*, 1104−1121.

(5) Dati, F.; Panteghini, M.; Apple, F. S.; Christenson, R. H.; Mair, J.; Wu, A. H. *Scand. J. Clin. Lab. Invest.* **1999**, *59*, 113−123.

(6) Wang, Y.; Yang, Y. Z.; Chen, C.; Wang, S. P.; Wang, H.; Jing, W. W.; Tao, N. J. *ACS Sens.* **2020**, *5*, 1126−1131.

(7) Yang, R.; Li, F.; Zhang, W. C.; Shen, W.; Yang, D.; Bian, Z. P.; Cui, H. *Anal. Chem.* **2019**, *91*, 13006−13013.

(8) Lou, D. D.; Fan, L.; Cui, Y.; Zhu, Y. F.; Gu, N.; Zhang, Y. *Anal. Chem.* **2018**, *90*, 6502−6508.

(9) Liu, X. H.; Wang, Y.; Chen, P.; McCadden, A.; Palaniappan, A.; Zhang, J. L.; Liedberg, B. *ACS Sens.* **2016**, *1*, 1416−1422.

(10) Su, Y. Y.; Wu, D.; Chen, J.; Chen, G.; Hu, N.; Wang, H. L.; Wang, P. X.; Han, H. Y.; Li, G. L.; Wu, Y. N. *Anal. Chem.* **2019**, *91*, 11687−11695.

(11) Lopa, N. S.; Rahman, M. M.; Ahmed, F.; Ryu, T.; Sutradhar, S. C.; Lei, J.; Kim, J.; Kim, D. H.; Lee, Y. H.; Kim, W. *Biosens. Bioelectron.* **2019**, *126*, 381−388.

(12) Chekin, F.; Vasilescu, A.; Jijie, R.; Singh, S. K.; Kurungot, S.; Iancu, M.; Badea, G.; Boukherroub, R.; Szunerits, S. *Sens. Actuators, B* **2018**, *262*, 180−187.

(13) Dhawan, S.; Sadanandan, S.; Haridas, V.; Voelcker, N. H.; Simon, B. P. *Biosens. Bioelectron.* **2018**, *99*, 486−492.

(14) Shanmugam, N. R.; Muthukumar, S.; Chaudhry, S.; Anguiano, J.; Prasad, S. *Biosens. Bioelectron.* **2017**, *89*, 764−772.

(15) Kumar, S.; Kumar, S.; Augustine, S.; Malhotra, B. D. *J. Mater. Res.* **2017**, *32*, 2966−2972.

(16) Yan, H. X.; Tang, X. D.; Zhu, X. D.; Zeng, Y. B.; Lu, X.; Yin, Z. Z.; Lu, Y. X.; Yang, Y. W.; Li, L. *Sens. Actuators, B* **2018**, *277*, 234−240.

(17) Lv, H.; Li, Y. Y.; Zhang, X. B.; Li, X. J.; Xu, Z.; Chen, L.; Li, D. G.; Dong, Y. H. *Biosens. Bioelectron.* **2019**, *133*, 72−78.

(18) Chen, Y.; Mei, L. P.; Feng, J. J.; Yuan, P. X.; Luo, X. L.; Wang, A. J. *Biosens. Bioelectron.* **2019**, *145*, No. 111638.

(19) Cote, A. P.; Benin, A. I.; Ockwig, N. W.; O'Keeffe, M.; Matzger, A. J.; Yaghi, O. M. *Science* **2005**, *310*, 1166−1170.

(20) Lohse, M. S.; Bein, T. *Adv. Funct. Mater.* **2018**, *28*, No. 1705553.

(21) Cai, L. H.; Hu, C. L.; Liu, S. N.; Zhou, Y.; Pang, M. L.; Lin, J. *Sci. China Mater.* **2021**, *64*, 488−497.

(22) Diercks, C. S.; Yaghi, O. M. *Science* **2017**, *355*, No. eaal1585.

(23) Ding, S. Y.; Gao, J.; Wang, Q.; Zhang, Y.; Song, W. G.; Su, C. Y.; Wang, W. *J. Am. Chem. Soc.* **2011**, *133*, 19816−19822.

(24) Furukawa, H.; Yaghi, O. M. *J. Am. Chem. Soc.* **2009**, *131*, 8875−8883.
(25) Zeng, Y. F.; Zou, R. Q.; Zhao, Y. L. *Adv. Mater.* **2016**, *28*, 2855−2873.
(26) Han, S. S.; Furukawa, H.; Yaghi, O. M.; Goddard, W. A. *J. Am. Chem. Soc.* **2008**, *130*, 11580−11581.
(27) Ma, Y. F.; Yuan, F.; Yu, Y.; Zhou, Y. L.; Zhang, X. X. *Anal. Chem.* **2020**, *92*, 1424−1430.
(28) Liu, X. L.; Pang, H. W.; Liu, X. W.; Li, Q.; Zhang, N.; Mao, L.; Qiu, M. Q.; Hu, B. W.; Yang, H.; Wang, X. K. *Innovation* **2021**, *2*, No. 100076.
(29) Liang, H.; Xu, H. B.; Zhao, Y. T.; Zheng, J.; Zhao, H.; Li, G. L.; Li, C. P. *Biosens. Bioelectron.* **2019**, *144*, No. 111691.
(30) Liu, T. Z.; Hu, R.; Zhang, X.; Zhang, K. L.; Liu, Y.; Zhang, X. B.; Bai, R. Y.; Li, D. L.; Yang, Y. H. *Anal. Chem.* **2016**, *88*, 12516−12523.
(31) Zhang, T.; Ma, N.; Ali, A.; Wei, Q.; Wu, D.; Ren, X. *Biosens. Bioelectron.* **2018**, *119*, 176−181.
(32) Liu, S. N.; Hu, C. L.; Liu, Y.; Zhao, X. Y.; Pang, M. L.; Lin, J. *Chem. - Eur. J.* **2019**, *25*, 4315−4319.
(33) Das, J.; Patra, S.; Yang, H. *Chem. Commun.* **2008**, 4451−4453.
(34) Ding, Y.; Zhang, X.; Liu, X.; Guo, R. *Langmuir* **2006**, *22*, 2292−2298.
(35) Wang, M. H.; Pan, Y. H.; Wu, S.; Sun, Z. W.; Wang, L.; Yang, J.; Yin, Y. M.; Li, G. X. *Biosens. Bioelectron.* **2020**, *169*, No. 112638.
(36) Wang, H. L.; Ning, X. K.; Wang, Z. J. *RSC Adv.* **2015**, *5*, 76783−76787.
(37) Chen, G. C.; Liu, C. H.; Wu, W. C. *Anal. Chim. Acta* **2021**, *1143*, 84−92.
(38) Zhang, T.; Chen, Y. L.; Huang, W.; Wang, Y.; Hu, X. Y. *Sens. Actuators, B* **2018**, *276*, 362−369.
(39) Shi, X. F.; Yao, Y. J.; Xu, Y. L.; Liu, K.; Zhu, G. S.; Chi, L. F.; Lu, G. *ACS Appl. Mater. Interfaces* **2017**, *9*, 7481−7488.
(40) Xu, H.; Gao, J.; Jiang, D. L. *Nat. Chem.* **2015**, *7*, 905−912.
(41) Ma, W. D.; Zheng, Q.; He, Y. T.; Li, G. R.; Guo, W. J.; Lin, Z.; Zhang, L. *J. Am. Chem. Soc.* **2019**, *141*, 18271−18277.
(42) Sangpour, P.; Akhavan, O.; Moshfegh, A. Z. *J. Alloys Compd.* **2009**, *486*, 22−28.
(43) Han, X.; Li, S. H.; Peng, Z. L.; Othman, A. M.; Leblanc, R. *ACS Sens.* **2016**, *1*, 106−114.

https://doi.org/10.1021/acs.analchem.1c02636
Anal. Chem. 2021, 93, 13572−13579